



SIMULATION OF AN INDUCTION MOTOR DRIVEN BY A MODULAR MULTILEVEL CASCADED INVERTER WITHOUT SPEED SENSOR WITH FUZZY CONTROLLER

¹B. NAGESWARA RAO, ²T.S. VIJAYALAKSHMI

¹Assistant Professor, ANURAG Group of Institutions (Formerly known as CVSR College of Engineering(Autonomous))Affiliated to JNTUH, Hyderabad, Telangana, India.

²MTech, ANURAG Group of Institutions (Formerly known as CVSR College of Engineering(Autonomous))Affiliated to JNTUH, Hyderabad, Telangana, India.

ABSTRACT—The main aim of this document is to validate the effectiveness and practicability of a speed-sensor less start-up process meant for a DSCC based induction motor drive, in which the motor-powered twitches rotate as of halt to mid speed by a slope change. This motor drive is apt mainly for a large-capacity fan- or blower-like load. The load torque is proportionate to a square of the motor mechanical speed. Here we are with the fuzzy regulator relate to other controller i.e. the fuzzy regulator is the utmost appropriate for the human decision-making means, run the function of an electronic arrangement with result of expert. The start-up method is characterized by combining capacitor-voltage control in the company of motor-speed control. The motor-speed control by the minimal stator current plays a vital role in eliminating a speed sensor from the drive structure and in dropping an ac voltage fluctuation happening across every dc capacitor. Numerous start-up waveforms illustrate steady presentation from stop to mid speed with dissimilar load torques. By means of the fuzzy Regulator for a nonlinear system permit for a decrease of indecisive special effects in the system control and progress the effectiveness. By means of the simulation outcomes we can verify that the motor-speed regulator planned for the DSCC-based drive system.

Index Terms—Medium-voltage induction motor drives, minimal stator current, modular multilevel cascade inverters, speed sensor less start-up method, Fuzzy logic controller.

I. INTRODUCTION.

A modular multilevel cascade inverter base on twofold star chopper cell (MMCI-DSCC) has been estimated as one of the next-generation medium-voltage multilevel pulse width modulation (PWM) inverters for such speed drive. The motor-speed control makes it achievable to remove a speed sensor from the drive system and to diminish the ac-voltage oscillation in all frequency arrays.

The motorspeed control makes it achievable to abolish a speed sensor from the drive system and to alleviate the ac voltage oscillation in all frequency range. This motor-speed control relies on a correspondent circuit of an induction motor, which was anticipated. By means of this document is to

validate the efficiency and achievability of a speed-sensor less start-up scheme for a DSCC based induction motor drive, in which the motor starts revolving from standstill to middle speed with a slope alteration. For the sake of ease, the MMCI-DSCC is referred to as the “DSCC” in this thesis. Every support of DSCC consists of two up and about and off-putting arms and a center-tapped inductor sit among the two arms. Each arm consists of manifold bidirectional dc/dc choppers call as “chopper cells.” The low voltage side of the chopper cells is associated in cascade, whereas the electrically balanced high-voltage side of chopper cells is outfitted by means of a dc capacitor and a voltage sensor.

As soon as a DSCC is applied to an ac motor drive, the DSCC would endure from ac-voltage fluctuations in the dc-capacitor voltages of every chopper cell in a low-speed assortment, because the ac-voltage oscillation gets more severe as a stator-current frequency gets lesser. Therefore, the oscillation must be attenuated acceptably to attain firm low-speed along with start-up performance.

This outcome in producing a reduced motor torque. A severe ac-voltage oscillation in a low-speed range can be mitigated by inserting a common-mode voltage along with superimposing a circulating current on each leg of the DSCC. in general, it is advantageous to remove a speed sensor from a motor drive, especially when a motor drive is introduced to a unfriendly surroundings, as soon as a new DSCC is applied to an already-existing line-started motor with no speed sensor, or as a lengthy lead cable is essential to fix a new DSCC by way of a new motor.

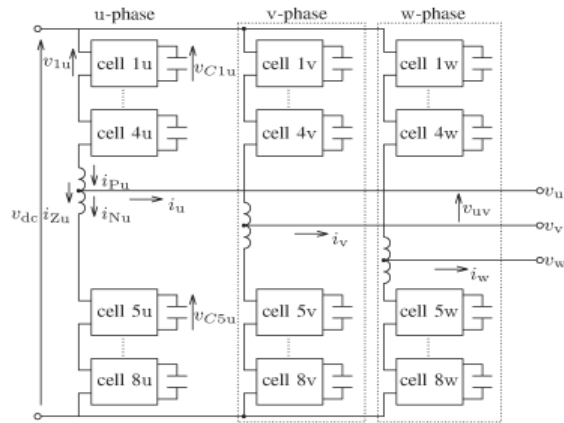
CASE STUDY OF PROPOSED THEORY

CIRCUIT CONFIGURATION AND CAPACITOR VOLTAGE CONTROL OF THE DSCC

A. Circuit Configuration

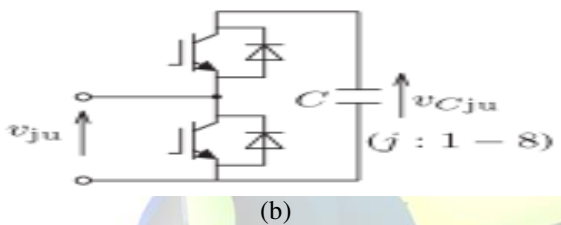
Fig.1 (a) demonstrates the major circuit configuration of the DSCC discussed in this thesis.

Every leg comprises of eight cascaded bidirectional chopper cells given away in Fig. 1(b) and a center tapped inductor per phase, as exposed in Fig. 1(c).

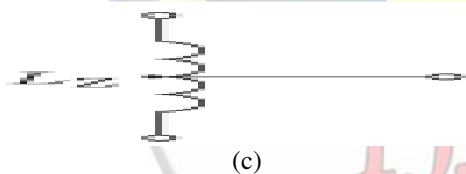


(a)

Fig. 1. Circuit configuration used for an MMCI-DSCC. (a) Power circuit.



(b)



(c)

Fig. 1. Circuit design for an MMCI-DSCC.

(a) Control circuit. (b) Chopper cell.

(c) Center-tapped inductor.

The middle tap of each inductor is coupled straight to each of the stator terminals of an induction motor; everywhere i_{iu} is the u-phase stator current. The center-tapped inductor is extra price efficient than two noncoupled inductors for each leg, as the centertapped inductor present inductance L_Z merely to the circulating current i_Z and no inductance to the stator current i_{iu} . This compensation in the center-tapped inductor is generally welcomed, for the greatest part applications to motor drives, in which no ac inductors be necessary connecting the motor along by means of the inverter. In Fig. 1, instantaneous currents i_{Pu} and i_{Nu} are the u-phase positive and negative-arm currents, correspondingly, and i_{Zu} is the u-phase circulating current define as follows:

$$i_{Zu} \triangleq \frac{1}{2}(i_{Pu} + i_{Nu}) \quad (1)$$

The individual ac components incorporated in the three-phase circulating currents i_{Zu} , i_{Zv} , and i_{Zw} evoke each other out, so that no ac component appear in either motor current or dc-link current.

The arm currents i_{Pu} and i_{Nu} can express as linear function of binary self-governing variables i_u and i_{Zu} as surveys:

$$i_{Pu} = \frac{i_u}{2} + i_{Zu} \quad (2)$$

$$i_{Nu} = -\frac{i_u}{2} + i_{Zu} \quad (3)$$

The dc-capacitor voltage in every chopper cell comprises of dc and ac components cause an ac-voltage oscillation. When neither common-mode voltage nor ac circulating current is superimpose, the peak-to-peak ac-voltage flux Δv_{Cju} is approximated as follows:

$$\Delta v_{Cju} \cong \frac{\sqrt{2}I_1}{4\pi fC} \quad (4)$$

Where I_1 is the rms value of the stator current, f is the frequency of the stator current, and C is the capacitance value of every dc capacitor. According toward Δv_{Cju} is inversely proportional to f as well as proportional to I_1 . Therefore, Δv_{Cju} rises as the stator-current frequency declines. [6] presented a short overview on widely used microwave and RF applications and the denomination of frequency bands. The chapter start outs with an illustrative case on wave propagation which will introduce fundamental aspects of high frequency technology.

- It disturbs the voltage rating of insulated-gate bipolar transistors.
- It origins more modulation to every chopper cell.
- It makes the arrangement unbalanced because the ac-voltage fluctuation can be considered as an interruption to the control system. As a result, the ac-voltage oscillation should be mitigated to an appropriate stage.

B. Capacitor-Voltage Control

Fig. 2 illustrates the over-all controller block figure of the startup process.

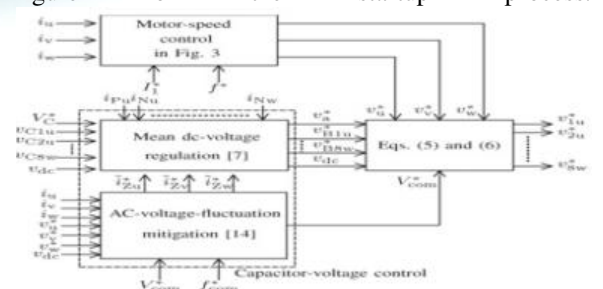


Fig. 2. Overall control block diagram for the start-up method.

This thesis employs two kinds of accessible capacitor-voltage control techniques for amendable mean dc voltage of every dc capacitor and for extenuating the ac-voltage fluctuation at the stator-current frequency. The mean dc-voltage regulation can be achieved by using the “arm” balancing control applied to the six arms and the “individual” balancing control applied to the one arm at the similar instance. This is able to diminish the ac-voltage oscillation at the stator-current frequency, hence leading to start up from standstill. The circulating-current response control incorporated in the mean dc-voltage parameter block yields a command voltage of $v^* \ast A$.

Lastly, command-phase voltages for every chopper cell, i.e., v^*_{ju} , are known as follows:

$$v^*_{ju} = v^*_a + v^*_{Bju} - \frac{v^*_u + v^*_{com}}{4} + \frac{v^*_{dc}}{8} \quad (j = 1 - 4) \quad (5)$$

$$v^*_{ju} = v^*_a + v^*_{Bju} + \frac{v^*_u + v^*_{com}}{4} + \frac{v^*_{dc}}{8} \quad (j = 5 - 8) \quad (6)$$

Now v^*_a and v^*_{Bju} are used to control the mean dc voltage, v^*_u is the command motor voltage given by Fig. 3 described in the later section, v^*_{com} is the command common-mode voltage, and v^*_{dc} is the dc-link voltage use as feedforward control. In addition, here is no association connecting common-mode voltage and power evaluation of the motor. This manuscript switches over the two capacitor-voltage control techniques according to the stator-current frequency as follows.

C. MOTOR-SPEED CONTROL

This segment describes a motor-speed control forming a feedback loop of three-phase stator currents for achieving a steady start-up of an induction motor. Primary, the motor-speed control is discussed in conditions of an appearance and purpose. Next, it is compared with conventional motor-speed control techniques, i.e., “volts-per-hertz” and “slip-frequency” control techniques.

A. Control Principles

The motor-speed control forms a feedback loop of three-phase stator currents to realize a stable establishes from idle. This requires the current sensors attach to the ac terminal. The stator current in single phase is considered by the parallel arm currents detected. For that reason, no further current sensor is essential. Fig. 3 shows the block figure designed for the motor-speed control.

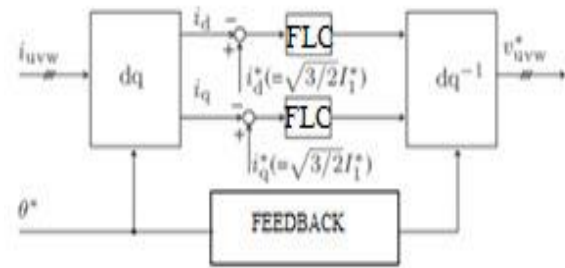


Fig. 3. Block figure for the motor-speed control based on a feedback control of the stator current.

Although the identical torque quantities by with the d-q conversion to improve current controllability. In Fig. 3, θ^* is the phase information used for the d-q transformation, whereas I^*_d and I^*_q be the control currents set by

$$i^*_d = i^*_q \sqrt{\frac{3}{2}} I^*_1 \quad (7)$$

Wherever I^*_1 is the control intended for the stator rms current. Note that I^*_1 and f^* are specified not by feedback control, however by feed forward control, as described later on. Fig. 4 shows a per-phase equivalent circuit of an induction motor based on the whole linkage flux of the secondary windings.

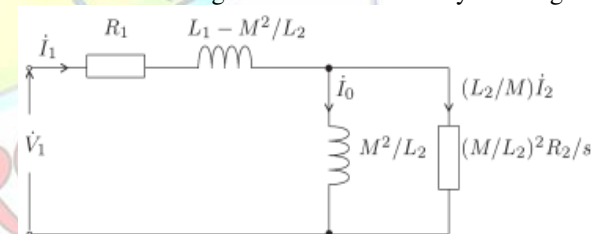


Fig. 4. Per-phase equivalent circuit based on the whole linkage flux of the secondary windings

Though this circuit is appropriate only underneath steady-state circumstances, it is appropriate to a fan- or blower-like load, in which the motor mechanical speed is attuned measured adequate to be measured as the steady-state situation. Here, I_1 is the phasor stator current, I_0 is the phasor magnetizing current, and I_2 is the phasor torque current. Note that I_0 and I_2 are orthogonal to everyone in steady-state circumstances. The rms value of I_1 , I_1 is given in Fig. 4 as follows:

$$I_1 = \sqrt{I_0^2 + \left(\frac{L_2}{M} I_2\right)^2} \quad (8)$$

The motor torque T_M is articulated by means of I_0 and I_2 to facilitate the rms standards of I_0 and I_2 , correspondingly, as follows:

$$T_M = 3PM I_0 I_2$$

Wherever P is the pole-pair numeral. Fig. 5 displays a phasor diagram for three poles apart

phasor stator currents I_{1i} , I_{1j} , and I_{1k} but by means of producing the similar torque, in which a relation of $I_{1i} < I_{1j} < I_{1k}$ holds. The imaginary frame I resembles to the magnetizing current I_0 , and the genuine frame R parallels to the torque current I_2 . It is vibrant in (9) and Fig. 5 that the motor torque T_M is proportionate to the area of the triangle bounded by I_1 , I_2 , and I_0 .

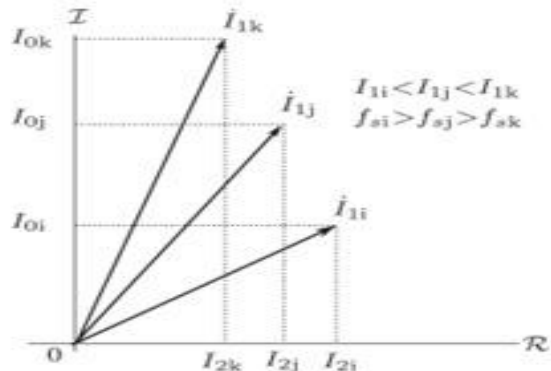


Fig. 5. Phasor diagram meant for the stator currents with dissimilar amplitudes

The slip frequency f_s is defined by resources of I_2 and I_0 as follows:

$$f_s = \frac{R_2 I_2}{2\pi M I_0} \quad (9)$$

B. Comparisons of Three Motor-Speed Control Techniques

The “volts-per-hertz” control or curtly “V/f” control has two self-governing variables V and f , in which V is the stator voltage and f is the stator frequency. Going on the further supply, the binary dependent variables be the stator current I_1 as well as the slip frequency f_s .

Table I summarizes comparisons amongst the three motorspeed control techniques, by means of a focal point on resemblance and divergence

Table I

comparison amongst existing volts-Per-Hertz And slip-Frequency control Techniques along with The projected motor-Speed control system

Independent Variables	v_s and f	v_s and f_s	I_1 and f
Dependent Variables	I_s and f_s	v_1 and f	v_1 and f_s
Voltage control	Feed forward		
Current control	-	feedback	feedback
Speed sensor	No	yes	NO

The slip-frequency control is able to give a quicker torque response than the V/f control as of the subsistence of a feedback control for the motor mechanical speed. The motor-speed control projected for the DSCC-based induction motor drive has binary self-governing variables I_1 and f , and the two reliant variables are V and f_s .

COMMAND STATOR CURRENTS

This sector describes how to establish the command of the stator rms current I^* and the stator-current frequency f^* . The subsequent two approaches can be used to establish I^* and f^* :

- Determination as of the equivalent circuit given away in Fig. 4;
- Determination from SIMULATIONS.

A. Design Considerations

- The utmost rate of each arm current is lesser than the amplitude of the rated stator current. The ac circulating current superimposed consequences in extenuating the ac-voltage fluctuation appearing across the dc capacitor of every chopper cell. For this reason, I^* be supposed to be minimized as the ac module of the arm current is relative to I^* .

B. Determination from the Equivalent Circuit Shown in Fig. 4

As soon as a speed-versus-load-torque attribute is recognized, the equivalent circuit shown in Fig. 4 is able to be used to decide I^* and f^* , along with the motor parameters as well as the moment of load inertia. The motor torque should gratify the following equation through the start-up:

$$T_M - T_L > (J_M + J_L) \frac{d\omega_{rm}}{dt} \quad (10)$$

Where T_L is the load torque, J_M is the moment of inertia of the motor, J_L is that of the load, and ω_{rm} is the mechanical angular velocity. The right-hand term on (11) corresponds to an acceleration torque for the start up. For making analysis simple and easy, the following reasonable approximations are made.

- The stator-current frequency f agrees well with its command f^* (i.e., $f = f^*$).
- The slip frequency f_s are much lesser than f (i.e., $f_s \ll f$).
- The moment of inertia of the load J_L is much larger than that of the motor J_M (i.e., $J_M \ll J_L$).

These three assumptions are applicable to fan- or blower-like loads for the subsequent reasons. The primary statement is appropriate since the motor frequency, or the motor mechanical speed, is attuned gradually, e.g., spending a small amount of or several proceedings to complete its start-up procedure. Lastly, (11) is simplified as follows:

$$T_M - T_L > J_L \frac{2\pi}{P} \frac{df^*}{dt} \quad (11)$$

Where $\omega_{rm} = 2\pi f^*/P$. Equation (12) means that the acceleration torque is proportional to the slope of change in f^* . The stator rms current essential to generate a motor torque gets the minimum when the next relation is met:

$$I_0 = \frac{L_2}{M} I_2 \quad (12)$$

Substituting (13) into (9) yields

$$I_2 = \sqrt{\frac{T_M}{3PL_2}} \quad (13)$$

Finally

I_1 is obtained by substituting (14) into (8) as follows:

$$I_1 = \sqrt{\frac{2L_2 T_M}{3PM^2}} \quad (14)$$

C. Determination from Simulations

The first value of I^*1 is deposit to nil. After that, I^*1 is being enlarged increasingly where the motor starts turning up. Lastly, Simulation tuning of the slope of I_1/f ($=I^*1/f$) is necessary to attain the steady start-up. The so-called “torque boost” role at small speeds, which is used in the V/f control, is applicable to the motor-speed control.

III. FUZZY LOGIC CONTROLLER

During FLC, crucial control accomplishment is determined by a set of linguistic rules. These rules are determined by the system. As the arithmetical variables be transformed into linguistic variables, numerical modeling of the scheme is not essential in FC.

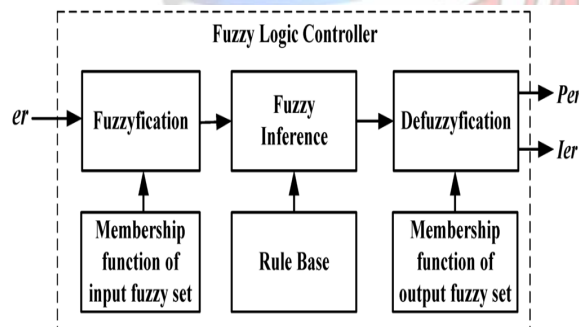


Fig.6.Fuzzy logic controller

The FLC comprises of three parts: fuzzification, interference engine and defuzzification. The FC is characterized as i. seven fuzzy groups for each input and output. ii. Triangular membership functions for simplicity. iii. Fuzzification by means of incessant creation of discourse. iv. Implication with Mamdani's, 'min' machinist. v. Defuzzification with the height method.

TABLE III: Fuzzy Rules

e	NB	NM	NS	ZE	PS	PM	PB
NB	NB	NB	NB	NB	NM	NS	ZE
NM	NB	NB	NB	NM	NS	ZE	PS
NS	NB	NB	NM	NS	ZE	PS	PM
ZE	NB	NM	NS	ZE	PS	PM	PB
PS	NM	NS	ZE	PS	PM	PB	PB
PM	NS	ZE	PS	PM	PB	PB	PB
PB	ZE	PS	PM	PB	PB	PB	PB

Fuzzification: Membership function standards are allocated to the linguistic variables, by means of seven fuzzy subsets: NB (Negative Big), NM (Negative Medium), NS (Negative Small), ZE (Zero), PS (Positive Small), PM (Positive Medium), and PB (Positive Big). The separation of fuzzy subsets and the shape of membership CE (k) E(k) function acclimatize the form up to appropriate system. The importance of input error and change in error are standardized by an input scaling factor. In this structure the input scaling factor has remained intended such that input values are sandwiched between and +1. The triangular shape of the membership function of this arrangement presumes that for some E (k) input there is only unique dominant fuzzy subset. The input error for the FLC is given as

$$E(k) = \frac{P_{ph(k)} - P_{ph(k-1)}}{V_{ph(k)} - V_{ph(k-1)}} \quad (15)$$

$$CE(k) = E(k) - E(k-1) \quad (16)$$

Inference Method: several composition approaches such as Max-Min and Max-Dot have been projected in the literature. In this thesis Min method is used. The output membership function of each regulation is specified by the smallest operator as well as maximum operator. Table 1 displays rule base of the FLC.

Defuzzification: while a plant usually needs a non-fuzzy charge of control, a defuzzification phase is required. To compute the output of the FLC, „height“ procedure is used and the FLC output alters the control output. More, the output of FLC wheels the switch in the inverter. In UPQC, the active power, reactive power, terminal voltage of the line and capacitor voltage are essential to be sustained. To establish these limitations, they are detected and related by means of the reference values. To attain this, the membership functions of FC are: error, modification in error and output

The set of FC rules are derivative from

$$u = -[\alpha E + (1-\alpha)C] \quad (17)$$

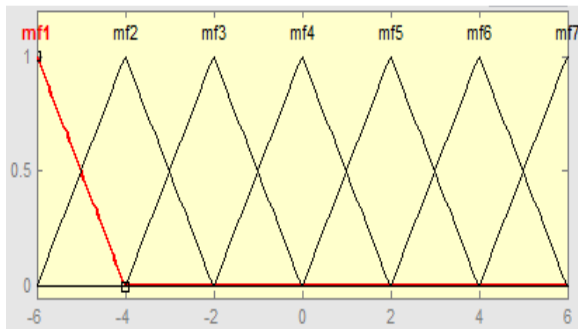


Fig 7 input error as membership functions

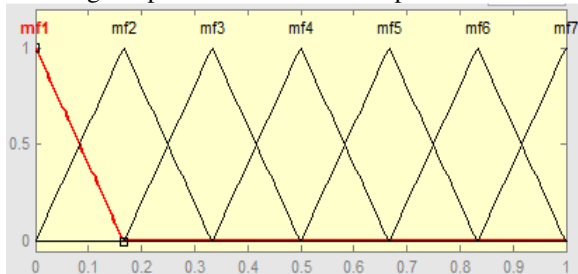


Fig 8 change as error membership functions

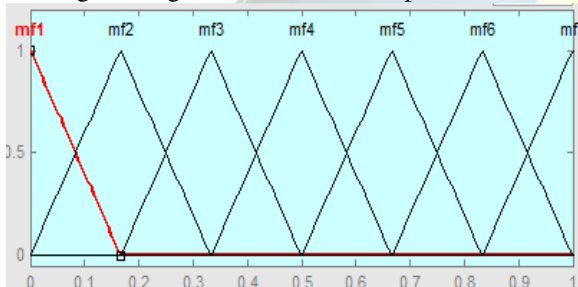


Fig.9 output variable Membership functions

Where α is self-adjustable factor which can control the whole process. E is the error of the system, C is the change in error and u is the controller variable.

SIMULATION

Chart II précise les limitations de circuit utilisées dans les SIMULATIONS.

Table III

Circuit constraints used in the SIMULATIONS

Rated active power		15kw
Rated line to line rms voltage	v_s	400v
Rated dc link voltage	V_{dc}	570v
Center tapped inductor	L_Z	4.0mH(12%)
DC capacitor of chopper cell	C	3.3mF
Dc capacitor voltage	V_c	140v
Unit capacitance constant	H	52ms(19)
Cell count per leg	N	8
Triangular wave carrier frequency	f_c	2Khz
Triangular wave carrier	f_c	2Khz

frequency		
-----------	--	--

A square-wave common-mode voltage as well as square wave circulating currents be used to diminish the ac-voltage oscillation of each dc capacitor, in which the rms value of the common-mode voltage V_{com} along with its frequency f_{com} be set to $V_{com}=180V$ and $f_{com}=50Hz$, correspondingly, for the subsequent reasons.

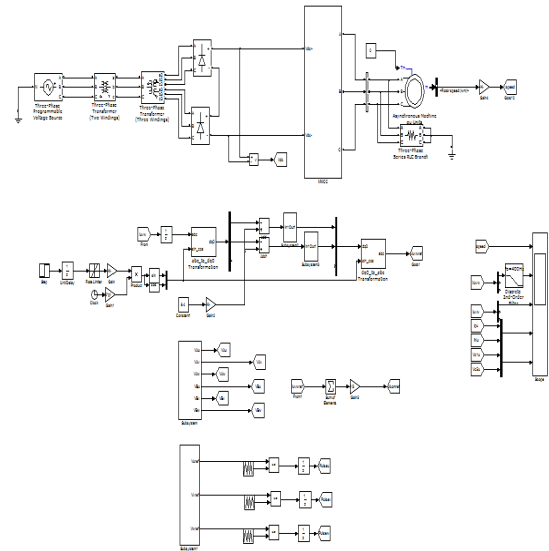


Fig. 10. Block diagram of simulation

- The command common-mode voltage V^*_{com} be put to build the modulation index of the DSCC be about unity.
- The command frequency f^*_{com} be set to be a smaller amount than one-tenth of the carrier frequency f_C (i.e., $f_{com} \leq f_C/10 = 200\text{Hz}$) to attain superior controllability of the ac circulating current.

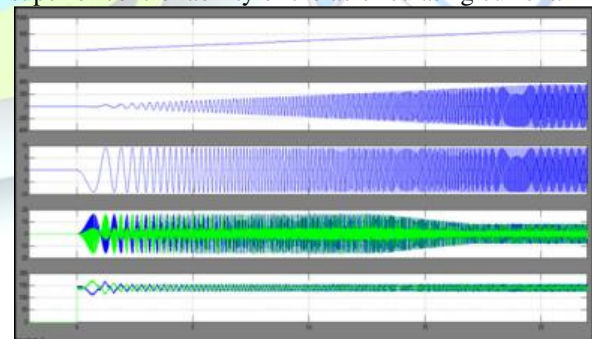


Fig. 11. Simulation start-up waveforms when $I^*_1=6.4$ A (20%) and $TL=0\%$, where $I_0=6.4$ A (35%)

The command for the stator rms current I^*1 in the motor speed control was determined by SIMULATIONS.

B. Start-Up Performance

Figs. 11–15 show Simulation start-up performance with dissimilar load torques. The harmonic voltages

included in the line-to-line voltage v_{uv} were eliminated by means of a low-pass filter with a cutoff frequency of 400 Hz.

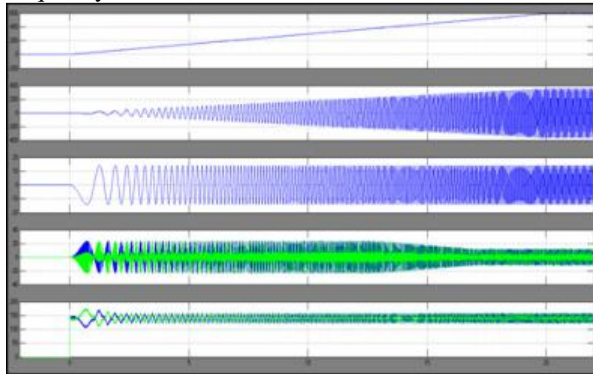


Fig. 12. Simulation start-up waveforms when $I^*1=10A$ (31%) and $TL=20\%$, where $I_0=7.0A$ (38%)

Fig.13 shows the Simulation start-up presentation with $TL=20\%$. Here, I^*1 was set to 17 a (53%), which is intended for evaluations with Fig. 8.

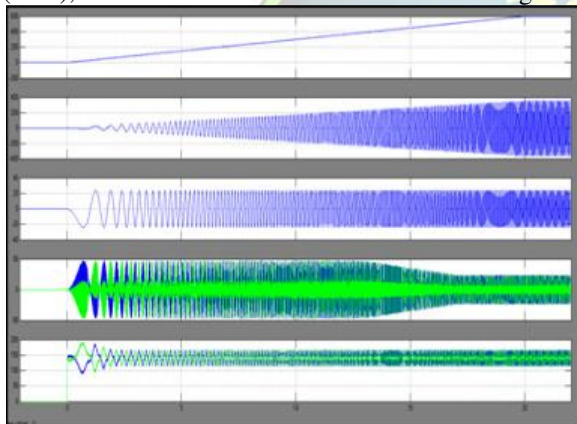


Fig. 13. Simulation start-up waveforms when $I^*1=17A$ (53%) and $TL=20\%$, where $I_0=16.6A$ (90%).

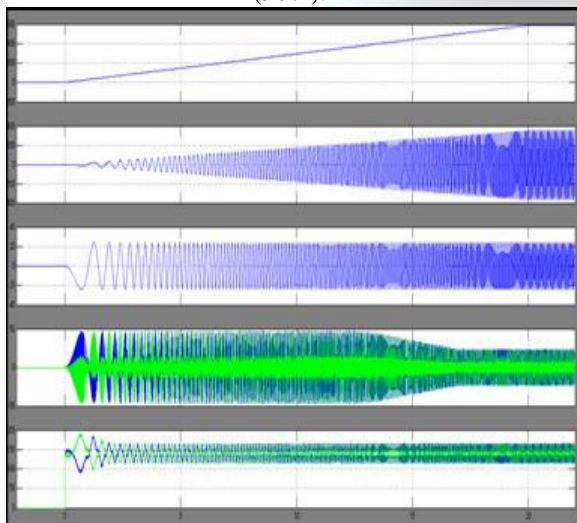


Fig. 14. SIMULATION start-up waveforms when $I^*1=14A$ (44%), and $TL=40\%$, where $I_0=9.9A$ (54%)

Fig.14 displays the Simulation start-up presentation with $TL=40\%$. Here, I^*1 was adjusted to $\sqrt{2}$ periods of that when $TL=20\%$, because I^*1 is proportionate to a square root of torque, rendering to (15).

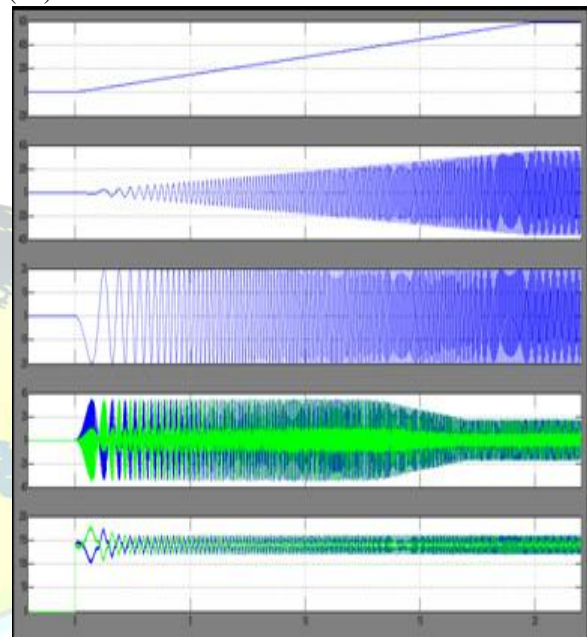


Fig. 15. Simulation start-up waveforms when $I^*1=17A$ (53%), and $TL=60\%$, where $I_0=12.0A$ (65%).

Fig. 15 shows the Simulation start-up performance with $TL=60\%$. Here, I^*1 was set to 17 A ($=\sqrt{3} \times 10A$, 53%). The magnetizing current I_0 reached 12.0 A ($=17A/\sqrt{2}$, 65%). The supreme amplitudes of the arm current and the peak-to-peak ac-voltage oscillation stood the same as those in Fig. 9, because I^*1 was conventional to the same value as Fig. 12.

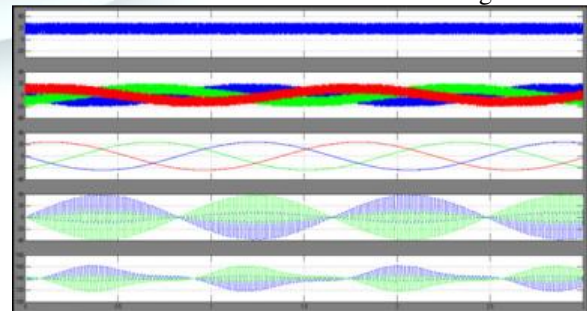


Fig. 16. Simulation steady-state waveforms when $I^*1=17A$ (53%), $f^*=1Hz$, and $TL=60\%$, where $I_0=12.0A$ (65%)

Fig. 17 displays those at $f^*=15Hz$. Here, V_{com} was condensed to 113 V, and the amplitude of the square-

wave circulating currents was condensed concurrently. The motor mechanical speed in addition the slip frequency was $N_{rm} = 438 \text{ min}^{-1}$ and $f_s = 0.4 \text{ Hz}$, correspondingly.

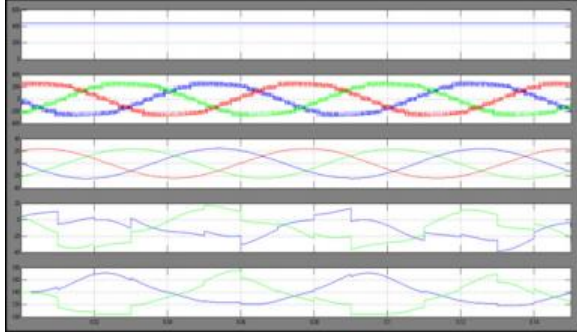


Fig. 17. SIMULATION steady-state waveforms when $I^* = 17 \text{ A}$ (53%), $f^* = 15 \text{ Hz}$, and $TL = 60\%$, where $I_0 = 12.0 \text{ A}$ (65%)

Fig. 18 shows those at $f^* = 20 \text{ Hz}$. Here, V_{com} and the amplitude of the square-wave circulating currents were abridged to nil, since the ac-voltage fluctuation of separately dc-capacitor voltage is not grave at this frequency. However the peak charge of the arm currents can continue concentrated to 19 A , which is 42%

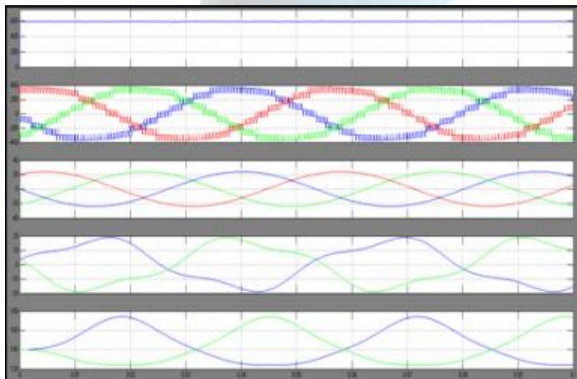


Fig. 18. SIMULATION steady-state waveforms with $I^* = 17 \text{ A}$ (53%), $f^* = 20 \text{ Hz}$, and $TL = 60\%$, where $I_0 = 12.0 \text{ A}$ (65%).

CONCLUSION

This thesis is to validate the efficiency and possibility of a speed-sensor less start-up method for a DSCC based induction motor drive, in which the motor jumps revolving from standstill to mid speed by means of a gradient variation. This start-up way is categorized by means of combining capacitor-voltage control in addition motor-speed control. At this juncture, we are using the fuzzy controller related to further controllers i.e. the fuzzy controller stands the utmost apt for the human decision-making mechanism, provided that the operation of an electronic system by choices of

professionals. The arm-current amplitudes in addition ac-voltage fluctuations diagonally each of the dc capacitors can be condensed to tolerable points. By means of using the fuzzy controller for a nonlinear system tolerates for a decrease of indeterminate properties in the scheme control and progresses the effectiveness. The start-up torque has continued increasing in a aspect of three, by no additional stress on equally arm currents as well as ac-voltage fluctuations.

REFERENCES

- [1] P. W. Hammond, "A new approach to enhance power quality for medium voltage ac drives," *IEEE Trans. Ind. Appl.*, vol. 33, no. 1, pp. 202–208, Jan./Feb. 1997.
- [2] R. Teodorescu, F. Blaabjerg, J. K. Pedersen, E. Cengcelci, and P. N. Enjeti, "Multilevel inverter by cascading industrial VSI," *IEEE Trans. Ind. Appl.*, vol. 49, no. 4, pp. 832–838, Jul./Aug. 2002.
- [3] J. Rodriguez, S. Bernet, J. O. Bin Wu, and S. Pontt, "Multilevel voltage source-converter topologies for industrial medium-voltage drives," *IEEE Trans. Ind. Electron.*, vol. 54, no. 6, pp. 2930–2945, Dec. 2007.
- [4] S. Malik and D. Kluge, "ACS 1000 world's first standard ac drive for medium-voltage applications," *ABB Rev.*, no. 2, pp. 4–11, 1998.
- [5] H. Akagi, "Classification, terminology, and application of the modular multilevel cascade converter (MMCC)," *IEEE Trans. Power Electron.*, vol. 26, no. 11, pp. 3119–3130, Nov. 2011.
- [6] Christo Ananth, [Account ID: AORZMT9EL3DL0], "A Detailed Analysis Of Two Port RF Networks - Circuit Representation [RF & Microwave Engineering Book 1]", Kindle Edition, USA, ASIN: B06XQY4MVL, ISBN: 978-15-208-752-1-7, Volume 8, March 2017, pp. 1–38.
- [7] M. Hagiwara and H. Akagi, "Control and SIMULATION of pulse-width modulated modular multilevel converters," *IEEE Trans. Power Electron.*, vol. 24, no. 7, pp. 1737–1746, Jul. 2009.
- [8] M. Hiller, D. Krug, R. Sommer, and S. Rohner, "A new highly modular medium voltage converter topology for industrial drive applications," in *Conf. Rec. EPE*, 2009, pp. 1–10.
- [9] S. Rohner, J. Weber, and S. Bernet, "Continuous model of modular multilevel converter with Simulation verification," in *Conf. Rec. IEEE ECCE*, 2011, pp. 4021–4028.
- [10] M. Hagiwara, K. Nishimura, and H. Akagi, "A medium-voltage motor drive with a modular multilevel PWM inverter," *IEEE Trans. Power Electron.*, vol. 25, no. 7, pp. 1786–1799, Jul. 2010.



B. NAGESWARA RAO

Completed B. Tech in Electrical & Electronics Engineering from ACET, Hyderabad and MTech in Power Electronics in 2010 from RGM College of Engineering Affiliated to JNTUA. Working as Assistant Professor at ANURAG Group

of Institutions (Formerly known as CVSR College of Engineering (Autonomous)) Affiliated to JNTUH, Hyderabad, Telangana, India. Area of interest includes **Electrical Power System, power electronics, electrical Machines and drives control.**



T.S. VIJAYALAKSHMI

Completed B. TECH in Electrical & Electronics Engineering in 2009 from Gates Institute of Technology affiliated to Jawaharlal University, ANANTAPUR and Pursuing MTech from ANURAG Group of Institutions (Formerly known

as CVSR College of Engineering (Autonomous)) Affiliated to JNTUH, Hyderabad, Telangana, India. Area of interest includes Power Electronics.

E-mail id: nurani.vijayalakshmi@gmail.com

IJARTET